Received: 8 August 2019 | Revised: 5 November 2019 | Accepted: 17 December 2019

DOI: 10.1002/tal.1704

RESEARCH ARTICLE

WILEY

Improving the wind-induced human comfort of the Beijing Olympic Tower by a double-stage pendulum tuned mass damper

Xin Chen[1] | Aiqun Li[2] | Zhiqiang Zhang[3] | Liang Hu[4] | Peng Sun[5] | Zhong Fan[6] | Xianming Liu[6]

[1]Jiangsu Province Key Laboratory of Structure Engineering, Suzhou University of Science and Technology, Suzhou, PR China

[2]Advanced Innovation Center for Future Urban Design, Beijing University of Civil Engineering and Architecture, Beijing, PR China

[3]School of Civil Engineering, Southeast University, Nanjing, PR China

[4]NatHaz Modeling Laboratory, University of Notre Dame, Notre Dame, Indiana

[5]Department of Civil and Environmental Engineering, University of Michigan, Ann Arbor, Michigan

[6]Fanzhong Structural Design Studio, China Architecture Design & Research Group, Beijing, PR China

Correspondence
Xin Chen, Jiangsu Province Key Laboratory of Structure Engineering, Suzhou University of Science and Technology, Suzhou, PR China.
Email: chenx@usts.edu.cn

Funding information
A Project Funded by the Priority Academic Program Development of Jiangsu Higher Education Institutions; Jiangsu Government Scholarship for Overseas Studies; Natural Science Foundation of Jiangsu Education Department, Grant/Award Number: 19KJA430019; Six Talent Climax Foundation of Jiangsu, Grant/Award Number: JZ-004; Natural Science Foundation of Jiangsu Province, Grant/Award Numbers: BK20161581, BK20181078; Natural Science Foundation of China, Grant/Award Number: 51408389

Summary

With five sub towers and a maximum height of 246.8 m, the Beijing Olympic Tower (BOT) is a landmark of Beijing. The complex structural properties and slenderness of the BOT render it prone to wind loading. As far as the wind-induced performance of this structure is concerned, this paper thus aims at a tuned mass damper-based mitigation system for controlling the wind-induced acceleration response of the BOT. To this end, the three-dimensional wind loading of various wind directions are simulated based on the fluctuating wind force obtained by the wind tunnel test, by which the wind-induced vibration is evaluated in the time domain by using the finite element model. A double-stage pendulum tuned mass damper (DPTMD), which is capable of controlling the long period dynamic response and requires only a limited space of installation, is optimally designed at the upper part of the tower. Finally, the wind-induced response of the structure with and without DPTMD is compared with respect to various wind directions and in both the time and frequency domains. The comparative results show that the wind-induced accelerations atop the tower with the wind directions of 45, 135, 225, and 315° are larger than those with the other directions. The DPTMD significantly reduces the wind-induced response by the maximum acceleration reduction ratio of 30.05%. Moreover, it is revealed that the control effect varies noticeably for the five sub towers, depending on the connection rigidity between Tower1 and each sub tower.

KEYWORDS

double-stage pendulum tuned mass damper, high-rise building, human comfort, multi-tower structure, vibration mitigation, wind-induced responses

1 | INTRODUCTION

With the increasing use of high-strength materials, lightweight floors, and curtain wall systems, the mass and stiffness of modern high-rise buildings and towers are decreasing.[1,2] Thus, they suffer from excessive wind-induced oscillations.[3,4] The undesirably excessive vibration may cause

not only the structural damage or failure but also the discomfort of occupants. Hence, very often, those structures may need specific measures to mitigate the wind-induced responses.[5] Generally, increasing the structural stiffness is effective in reducing dynamic response, but it is often economically inefficient. Structural control technology, which aims to enhance structural safety and serviceability against dynamic excitations, is now a widely-used alternative.[6–10]

A tuned mass damper (TMD) is one of the simplest and most practical control devices and is especially useful in mitigating dynamic response within the narrow frequency range. Generally, a typical TMD can be modeled as a device consisting of a mass element, a stiffness element, and a damping element. The frequency of the TMD is tuned to a particular vibration frequency so that when the structural vibration at that frequency is excited, the damper will resonate out of phase and mitigate the induced vibration. A portion of vibration energy input to the structure may be imparted to the TMD and dissipated by the damping element. Due to the convenient implementation procedure, low cost, and nonrequirement of external energy, the TMD has attracted many researches, most of which are focused on the configuration, design, and application of the TMD. A proper configuration is essential to realize the TMD in engineering practice. Options of the effective stiffness may include the springs,[11,12] the suspended pendulum,[13,14] and the laminated rubber bearings.[15] Although the oil dampers are typical, there are still others such as the friction (Chung et al. 2013[16]), the eddy current,[17] the sub tuned absorbers,[18] and the pounding.[19,20] Moreover, the analysis and design methods of TMD are under active investigation, including the design formulas of the TMD's parameters. These researches may date back to Den Hartog,[21] such as simplified expressions for optimum TMD parameters of undamped/damped systems considering various combinations of responses (e.g., displacement, velocity, acceleration, and force) and excitations (e.g., harmonic and white noise random excitations[22–24]; Chung et al. 2013[25–27]). On the other hand, the metaheuristic optimization methods have been utilized in the design of the TMD.[28–33]

With the development in the past 4 decades, the TMD has been successfully installed on practical buildings to mitigate dynamic responses including pedestrian-induced vibration,[11,34] wind-induced vibration,[1,13] and earthquake-induced vibration.[3,27] Researches and applications show that the TMD in the high-rise tower can suppress the wind-induced vibration significantly, such as John Hancock Tower in Boston,[35] Taipei 101 Tower,[36] Shanghai Tower,[37] and many others.[1,4,12,13,38,39] Most of these cases are a TMD on a single-tower building, but most recently some complicated buildings with two or more towers have been constructed out of their architecture benefits. However, the researches of the TMD on these irregular buildings are rare. Hence, further investigations on the wind-induced vibration and mitigation are still needed for multi-tower buildings.

With a height of 246.8 m, Beijing Olympic Tower (BOT) in the northern of Beijing, China, is a new landmark. The BOT consists of five towers each of which has an atop large mass. Preliminary studies demonstrate that the upper part of the tower suffers from excessive wind-induced acceleration beyond the human comfortability limit. This paper presents a study on the TMD installed on the BOT. The remainder of this paper is organized as follows. Section 2 introduces the structural system of the BOT. Section 3 presents the finite element model (FEM) of the structure and discusses its dynamic characteristics. The following section introduces the results of the wind tunnel test for this structure and the simulation of the wind loading in the time domain. Section 5 designs a double-stage pendulum tuned mass damper (DPTMD) for this tower and assesses the mitigation effect of the tower by comparing the acceleration response with and without the DPTMD. Finally, the main conclusions of the numerical study are summarized in Section 6.

2 | DESCRIPTION OF THE BEIJING OLYMPIC TOWER

The BOT, shown in Figure 1, is adjacent to the landscape avenue on the axis line of the Beijing Olympic Forest Park. It boasts one of the two buildings around the world that is officially with Olympic rings permanently on the top.[40,41] This tower consists of five sub towers with different heights: one central tower (Tower1) located in the middle and four lower towers (Tower2, Tower3, Tower4, and Tower5) standing around

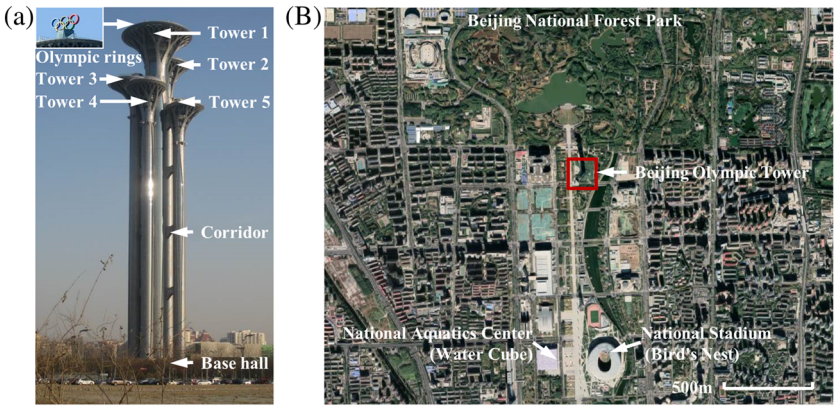

FIGURE 1 Building exterior and location of the Beijing Olympic Tower: (a) Building exterior. Building exterior and location of the BOT: (b) Building location

Tower1. The geometry of these sub towers is shown in Table 1. Towers 2–5 are connected to Tower1 by the corridors that are spatial steel girders with a height of 3.0 m and a width of 2.7 m. The sections of these sub towers are regular hexagons or circles, the dimensions of which increase with the height. The structure of Tower1 is a tube-in-tube system; its outer tube is composed of 16 concrete-filled steel tube circular columns stiffened by I-shape steel beams and H-shape steel braces. Towers 2–5 have their structures of tube systems composed of 6 concrete-filled steel tube circular columns connected by steel beams and braces.

3 | DYNAMIC CHARACTERISTICS OF THE STRUCTURE

3.1 | Finite element model

As shown in Figure 2, a three-dimensional FEM of the BOT was established by using Computers and Structures, Inc SAP2000 based on the structural design drawings. Two kinds of elements were employed in the FEM: the beam elements for the beams, columns, and braces and the shell elements for the floors and walls. The nonstructural components were modeled as the dead loads, whereas the mass was transformed from the dead loads and live loads. The connections between the braces and other components were hinged constraints, and the connections between the beams and columns and between the structure and its foundation were fixed constraints.

3.2 | Natural frequencies and modal shapes

The structural dynamic characteristics of the BOT were analyzed and shown in Table 2 and Figure 3. Here, 45° and 135° denotes the angles between the vibration directions and the *x*-axis in the *x*–*y* plane. It can be observed that the first natural period can be as long as 5.687 s and the torsional-translation period ratio is 0.775. The first two modes of the tower are overall bending in the direction of 45 and 135°, respectively, whereas the third mode is torsional. The first six modes are overall vibration modes, indicating that the corridors in this tower are stiff enough to combine the five sub towers. The modes from the sixth to ninth are all 2nd order torsional modes with different vibration shapes of the sub towers with dense-distributed frequencies, which may influence the vibration of the tower.

TABLE 1 Structural geometry of the Beijing Olympic Tower

Tower	Tower1	Tower 2	Tower 3	Tower 4	Tower 5
Architectural diameter/m	16.20	9.60	9.60	8.30	8.30
Structural diameter/m	14.00	7.30	7.30	6.00	6.00
Structural height/m	244.35	228.00	210.00	198.00	186.00
Slenderness ratio	17.45	31.23	28.77	33.00	31.00
Diameter of the top/m	51.20	33.60	32.40	30.00	26.40
Distance to Tower1/m	-	19.17	15.75	15.10	16.90

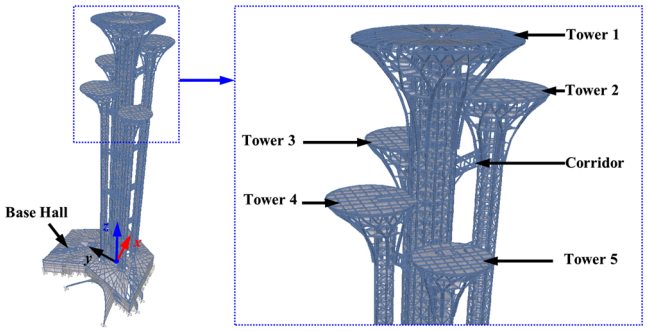

FIGURE 2 Finite element model of the BOT

TABLE 2 Natural frequencies of the tower

Modes	Frequency/Hz	Description
1	0.176	1st overall bending (45°)
2	0.181	1st overall bending (135°)
3	0.227	1st overall torsional (anti-symmetric bending of the Tower2 and 4 [45°] + anti-symmetric bending of the Tower3 and 5 [135°])
4	0.512	2nd overall bending (45°)
5	0.559	2nd overall bending (135°)
6	0.598	2nd overall torsional (symmetric bending of the Tower2 and 4 [45°] + anti-symmetric bending of the Tower3 and 5 [135°])
7	0.703	2nd overall torsional (symmetric bending of the Tower2 and 4 [45°] + symmetric bending of the Tower3 and 5 [135°])
8	0.721	2nd overall torsional (anti-symmetric bending of the Tower2 and 4 [45°] + symmetric bending of the Tower3 and 5 [135°])
9	0.790	2nd overall torsional (local vibration of the Tower4 crown + anti-symmetric bending of the Tower3 and 5 [135°])
10	1.019	3rd overall bending (45°)
11	1.088	3rd overall bending (135°)

4 | WIND LOADS SIMULATION

4.1 | Introduction of the wind tunnel test

Wind tunnel testing is an effective tool to evaluate the wind effects on buildings, especially those with complex silhouettes. In this study, wind tunnel tests of wind pressure on the BOT were carried out in the atmospheric boundary layer wind tunnel TJ-2 at Tongji University using a synchronous multipressure sensing system.[42] The dimension of the working section of the wind tunnel is 3.0 m wide and 2.5 m high. In order to reproduce the building shape as more detailed, the rigid sectional models are used. The whole building is divided into four sections vertically. The sectional models are made of plexiglass and acrylonitrile butadiene styrene. These four scaled segments are shown in Figure 4a, and the tower bodies and the tower crowns are scaled 1:70 and 1:100, respectively. The wind direction is defined as an angle from the tower south along a clockwise direction (see Figure 4b), and the measurements were made with the wind direction varying from 0 to 360° with the increment of 15°. 1,944 pressure taps were installed on these four sectional models. Due to the lack of instruments, the scales are divided into eight synchronous pressure-measuring segments, and not all of them use the same sampling rate. Hence, the pressure data were acquired at five sampling rates with a sampling length of 6,000 steps. The sectional model testing was conducted in a turbulent wind field with the turbulence intensity in Table 3, but the mean wind speed was 12.0 m/s and constant along the height. In this experiment, significant mutual aerodynamic interference effects among the sub towers existed, and complicated wind pressure, and force distributions were found. Therefore, the wind loads for the BOT are undoubtedly different from the conventional high-rise towers.

4.2 | Simulation of the three-dimensional wind loads

In this paper, because of the nonlinearity of the damping devices, the time-domain method is introduced to compute the wind-induced vibration of the BOT. To this end, one should simulate a three-dimensional wind loading field that is applicable to the FEM of the BOT firstly. In this study, the fluctuating wind pressure coefficients given by the wind tunnel tests are used to model the three-dimensional wind field. However, there are some difficulties to utilize these data directly: (a) as mentioned above, the data were acquired at five different sampling rates, including 6.0391, 8.1145, 7.3379, 6.8065, and 6.2723 Hz. (b) The directions of the tested wind pressure coefficients are perpendicular to the model surfaces. (c) There are 1,944 pressure taps and 6,000 steps per testing wind direction, and locations of the pressure taps do not strictly coincide one-to-one with the structural nodes in the FEM. These difficulties may lead to unsynchronized time steps, difficulty in the loads' assignment, and extensive computing time in the FEM time history analysis. Therefore, a method for the three-dimensional wind loading field simulation is proposed as depicted by Figure 5 including four steps:

1. In order to unify the sampling rates of all data into 6.0391 Hz, the nearest interpolation method is used. Figure 6 shows the comparison of the data from a pressure tap with and without interpolation and illustrates a good agreement not only in the time domain but also in the frequency domain.

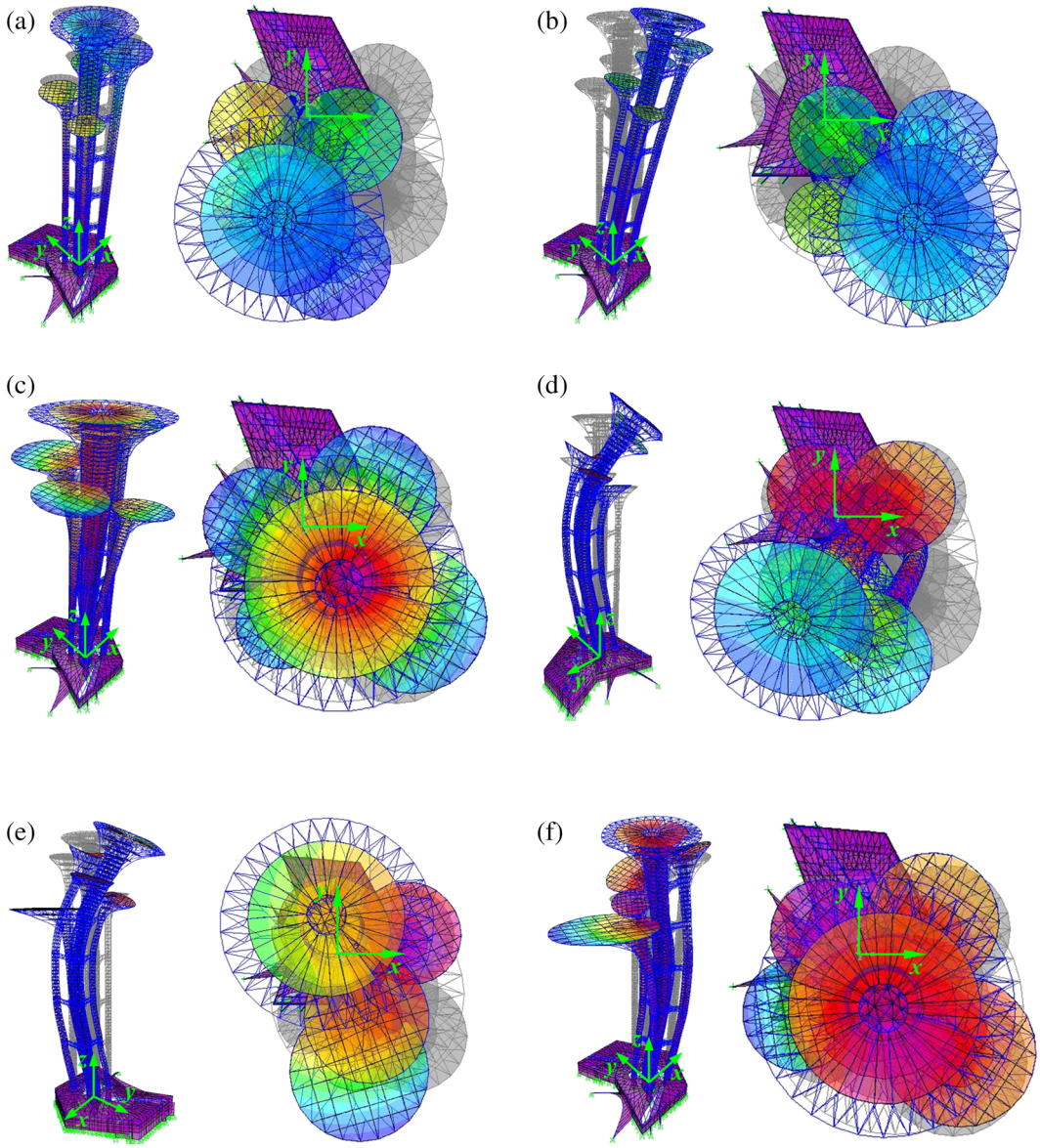

FIGURE 3 Modal shapes of the tower: (a) 1st mode. Modal shapes of the tower: (b) 2nd mode. Modal shapes of the tower: (c) 3rd mode. Modal shapes of the tower: (d) 4th mode. Modal shapes of the tower: (e) 5th mode. Modal shapes of the tower: (f) 6th mode

2. The wind pressure coefficients are decomposed into three orthogonal directions based on the global coordinate system of the FEM. Hence, the wind pressure coefficients in the *x*, *y*, and *z*-directions of global coordinates can be obtained as follows:

$$\mu_{si,x}(t) = \mu_{si}(t)\cdot\cos\varphi\cdot\sin\theta \tag{1}$$

$$\mu_{si,y}(t) = \mu_{si}(t)\cdot\cos\varphi\cdot\cos\theta \tag{2}$$

$$\mu_{si,z}(t) = \mu_{si}(t)\cdot\sin\varphi \tag{3}$$

where μ_{si} is the wind pressure coefficient of the *i*th pressure tap; $\mu_{si,x}$, $\mu_{si,y}$, and$\mu_{si,z}$ are the decomposed wind pressure coefficients in the *x*, *y*, and *z*-directions of the *i*th pressure tap; φ and θ, shown in Figure 5, are the angles between the normal direction of the surface and the horizontal and vertical axis directions, respectively.

3. The surface of the tower is divided into 1,367 subareas in which the values of the wind pressure coefficients of the embodied pressure taps are regarded as the same. In each subarea, the nominal wind pressure coefficients can be calculated as

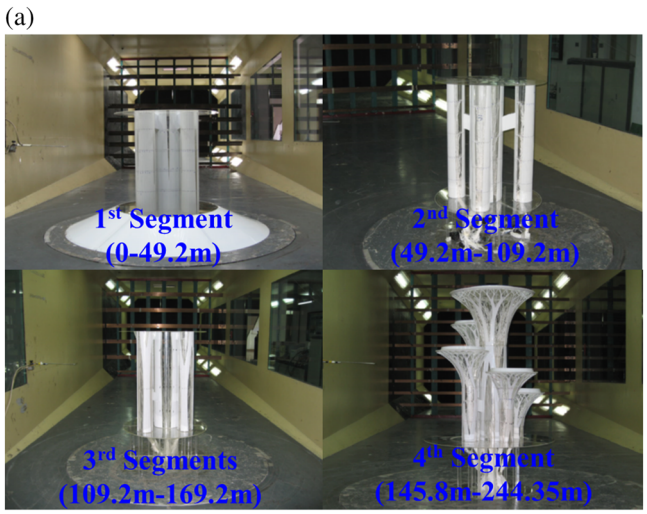

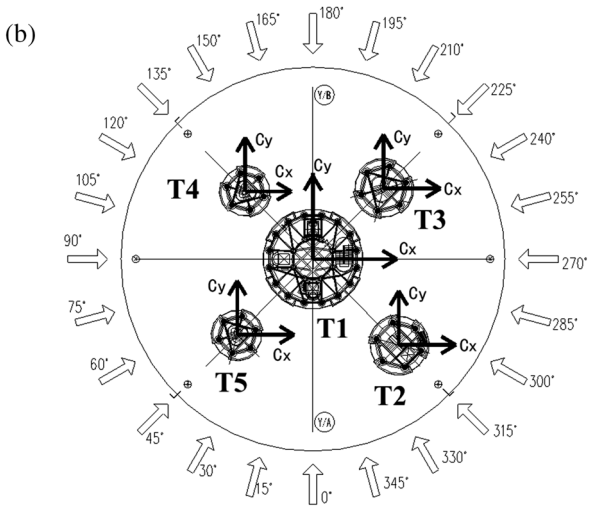

Note: T is short for Tower.

FIGURE 4 Wind tunnel tests: (a) Rigid segment models. Wind tunnel tests: (b) Definition of the wind direction

TABLE 3 Simulated turbulence intensity in the model tests

Segment model	Elevation/m	Reference height/m	Reference turbulence intensity/%	Simulated turbulence intensity/%
1	0–49.2	30–40	18–20	18
2	49.2–109.2	70–90	15–16	15
3	109.2–169.2	130–150	13–14	14
4	145.8–244.35	180–200	12	11.5

$$\mu_{sk} = \frac{\sum_{i=1}^{n} A_i \mu_{si}}{\sum_{i=1}^{n} A_i} \tag{4}$$

where μ_{sk} is the wind pressure coefficient of the kth subarea, A_i is the influence area of ith pressure tap, and n is the total number of the pressure taps included in the kth area. Then the wind pressure of the kth subarea can be written as

$$w_k(t) = \mu_{sk}(t)\mu_{zk}w_0 \tag{5}$$

where w_k is the wind pressure of the kth subarea, μ_{zk} is the height coefficients of the wind pressure, and w_0 is the basic wind pressure; in this study, w_0 = 0.30 *kPa* according to a 10-year return period.[43] Both Equations (4) and (5) apply to x, y, and z-directions.

4. Lastly, the loading nodes in the FEM are selected for the subareas in Step (3), and the wind loading time histories can be calculated as

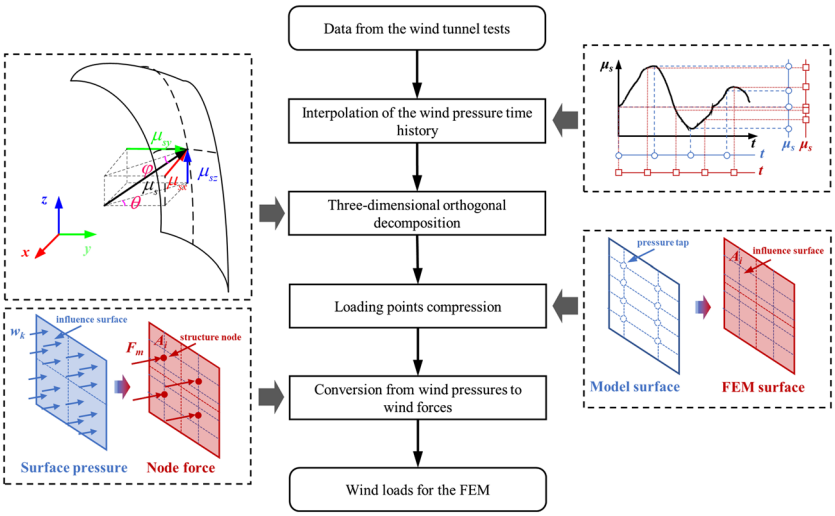

FIGURE 5 Flowchart for the three-dimensional wind field simulation

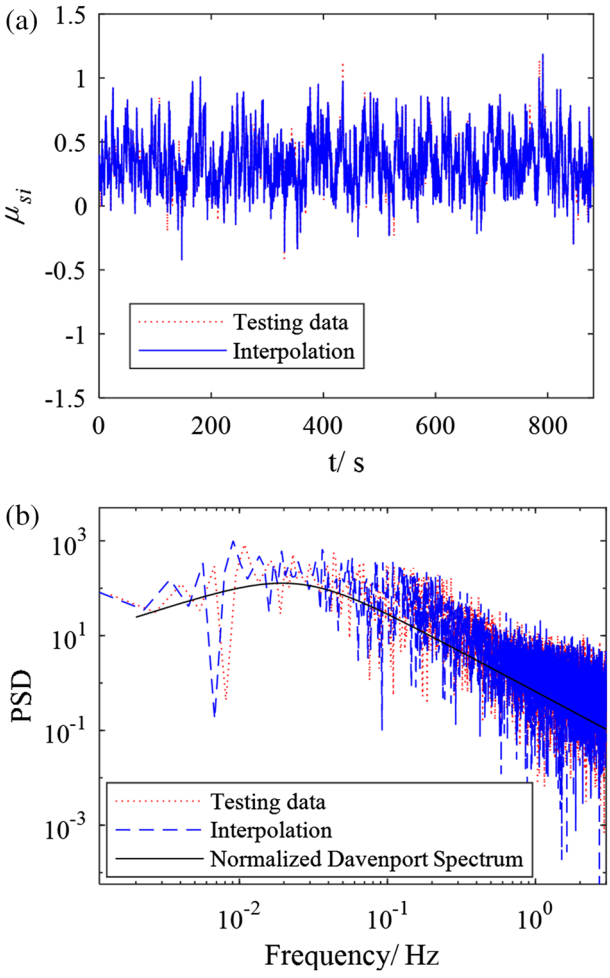

FIGURE 6 Comparison between data without and with interpolation: (a) Time history of the wind pressure coefficient. Comparison between data without and with interpolation: (b) Power spectrum density of the wind pressure coefficient

$$F_m(t) = w_k(t)A_m \tag{6}$$

where F_m is the mth loading nodes, and A_m is the influence area of the mth loading nodes. Finally, 4,101 time histories in FEM global coordinate system are obtained.

5 | VIBRATION CONTROL USING DPTMD

5.1 | Design of the double-stage pendulum tuned mass damper

A TMD system is installed in the BOT in order to mitigate the excessive wind-induced vibration. Constrained by the architectural requirements, the space available for the mitigation service in this building is quite limited: only a room of 4.80 × 4.20 × 5.80 m can be utilized. In order to take full advantage of the space without a significant increase in the total weight, the fire water tank is utilized as the mass element of the absorber because the volume of the tank excludes the possibility as a sloshing-based mitigation. In consideration of all these factors, a DPTMD was designed and installed on the floor of the Tower1 at the height of 232.5 m (Figure 7).

There are some requirements, including long periods, limit space, and all motion directions, for the TMD used in this tower. If a conventional pendulum TMD scheme was used in this project, at least a space with more than 7.90 m in height should be needed. However, the height of the available space for the TMD is only 5.80 m. Therefore, this DPTMD system utilizes the fire water tank as the mass element and hangs the tank by

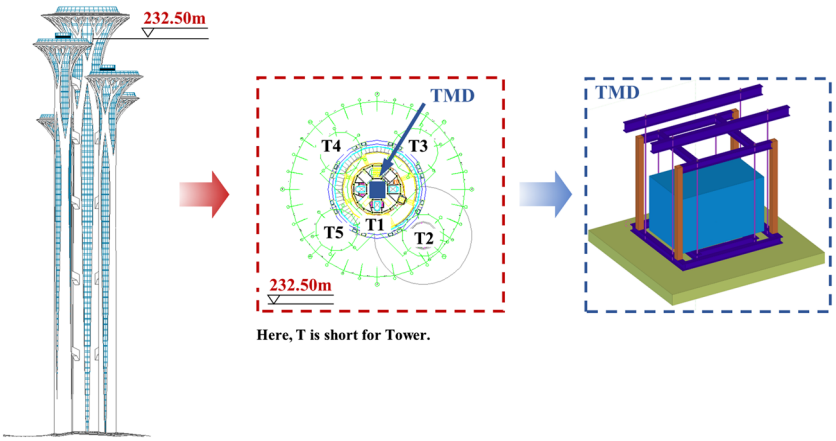

FIGURE 7 Position of the double-stage pendulum tuned mass damper in elevation and plane

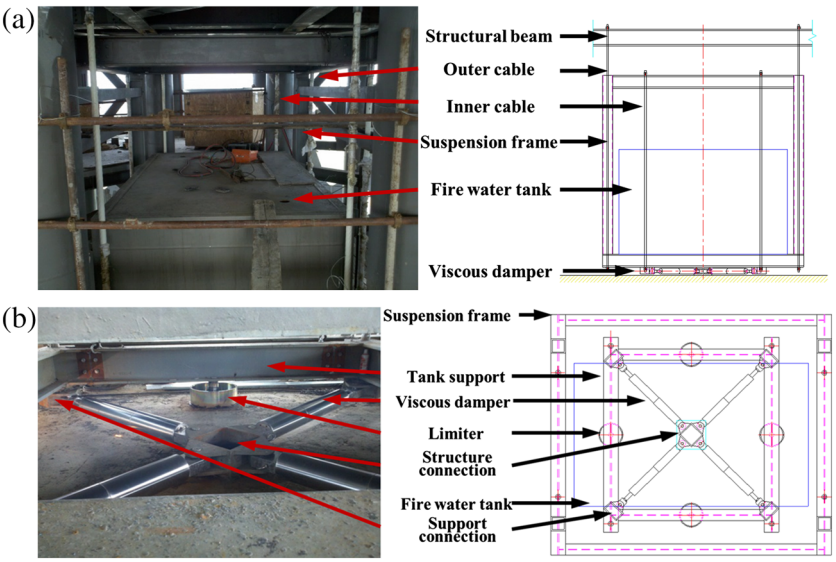

FIGURE 8 Configurations of the double-stage pendulum tuned mass damper (DPTMD): (a) Elevation view. Configurations of the DPTMD: (b) Plane view

TABLE 4 Parameters of the double-stage pendulum tuned mass damper system

Direction	*x*	*y*
Effective length of cable/m	7.90	7.90
Mass/t	50	50
Damping exponent of the damper	1	1
Damping coefficient of the damper/N·s/m	6,997	6,788

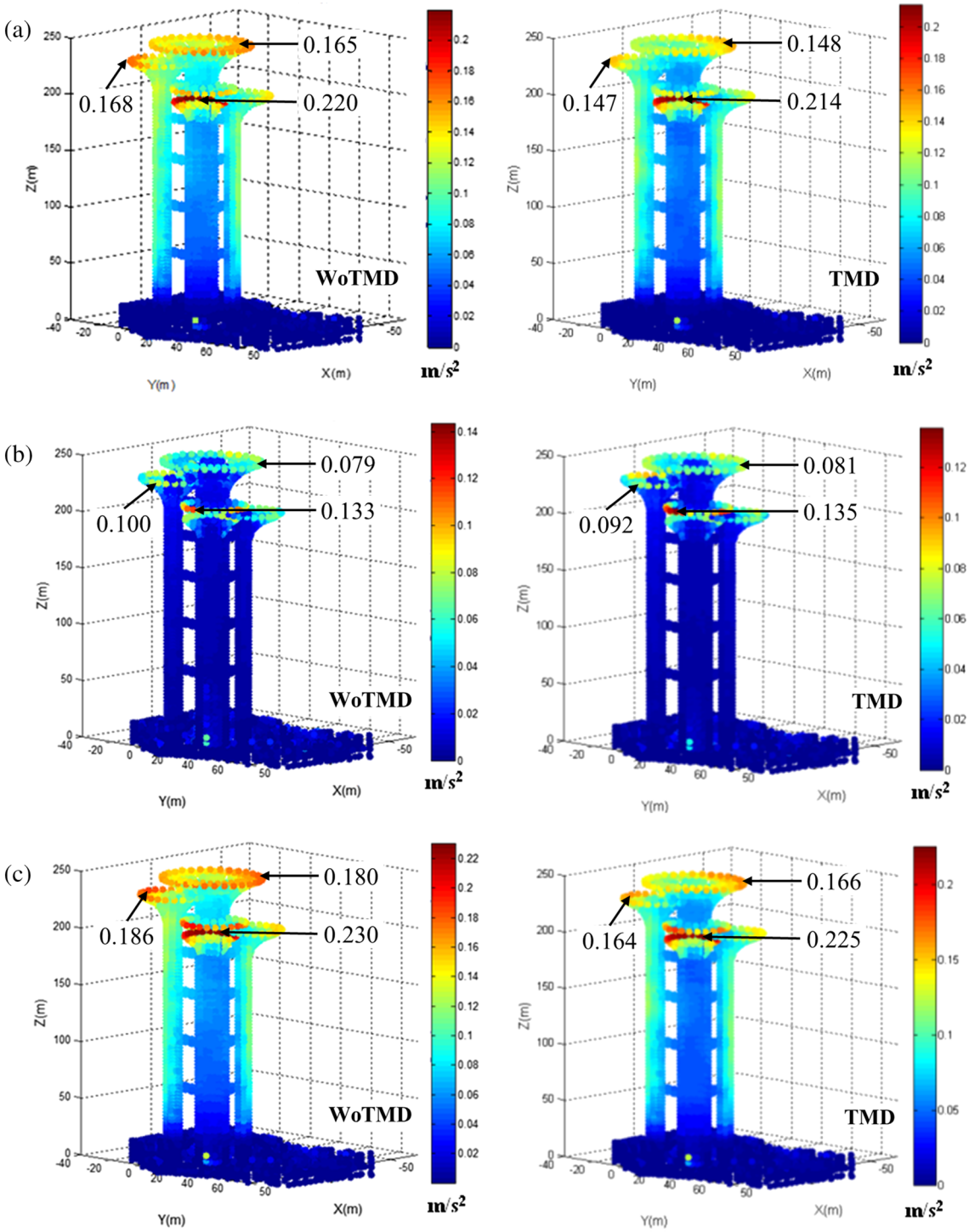

FIGURE 9 Wind-induced node accelerations of the BOT in 3-D space with the wind angles of 45° and 135°: (a) Summary accelerations of the horizontal directions (Wind direction: 45°). Wind-induced node accelerations of the BOT in 3-D space with the wind angles of 45° and 135°: (b) Vertical accelerations (Wind direction: 45°). Wind-induced node accelerations of the BOT in 3-D space with the wind angles of 45° and 135°: (c) Summary accelerations of the three directions (Wind direction: 45°). Wind-induced node accelerations of the BOT in 3-D space with the wind angles of 45° and 135°: (d) Summary accelerations of the horizontal directions (Wind direction: 135°). Wind-induced node accelerations of the BOT in 3-D space with the wind angles of 45° and 135°: (e) Vertical accelerations (Wind direction: 135°). Wind-induced node accelerations of the BOT in 3-D space with the wind angles of 45° and 135°: (f) Summary accelerations of the three directions (Wind direction: 135°). TMD, tuned mass damper; WoTMD, responses without TMD

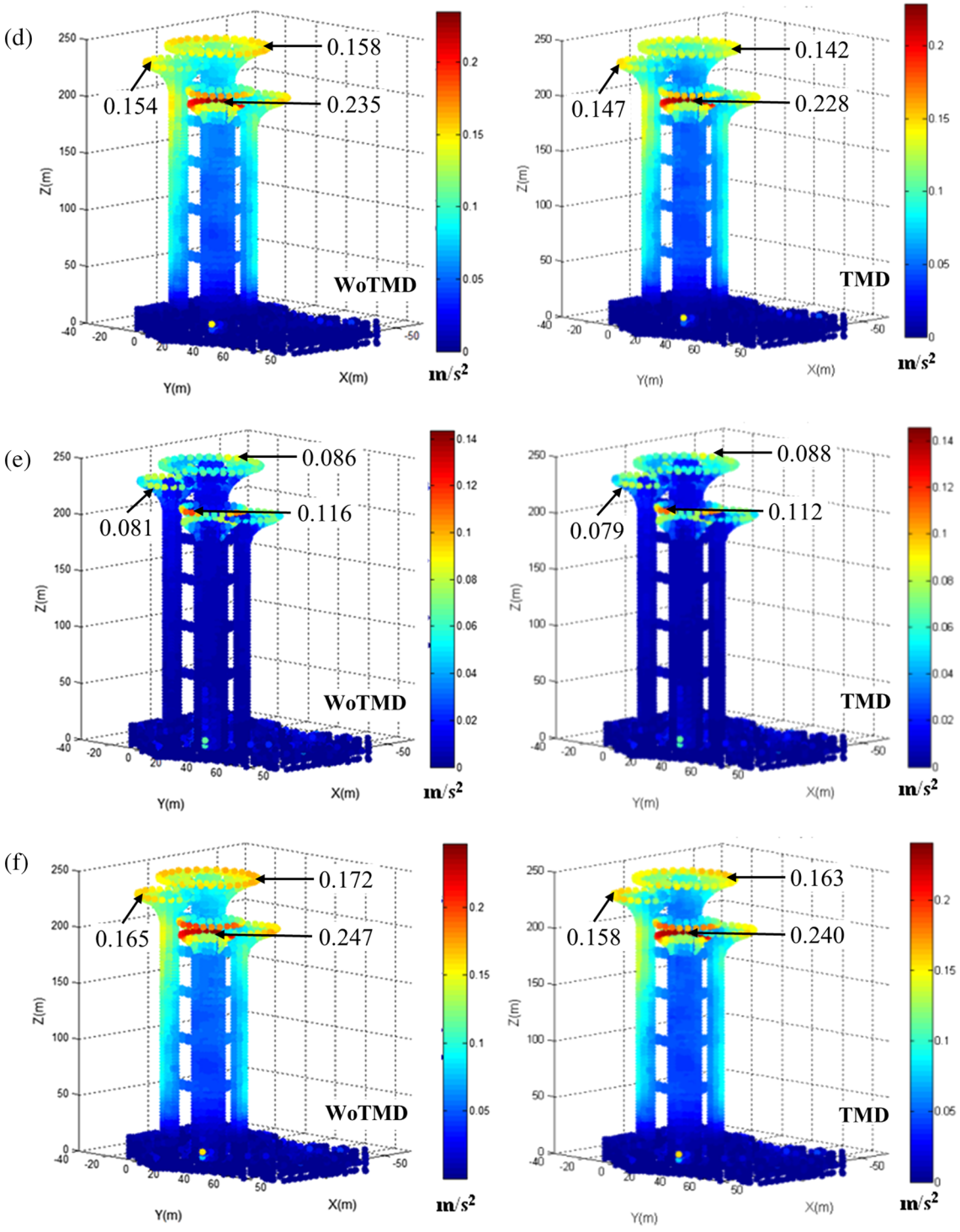

FIGURE 9 (Continued)

a double-stage suspension system. As shown in Figure 8, this system is composed of the fire water tank, outer cables, inner cables, suspension frame, tank support, viscous dampers, limiters, structure connections, and support connections. The tank support supports the fire water tank, which has a total mass of 50 t. They together are hung by the double-stage suspension system consisting of the outer cables, inner cables, and suspension frame. Four viscous dampers are installed between the floor and the tank support to suppress the motion between the tank and its support. Moreover, four limiters are used to restrict the maximum displacement of the tank. The parameters of the DPTMD are shown in Table.4, determined by the limitations of the total mass, maximum stroke, and installation space of the DPTMD. The mass ratio of the DPTMD to the structure is only 0.058%. The frequency ratio of the DPTMD in the directions of the first two modes are 1.055 and 1.025, whereas the

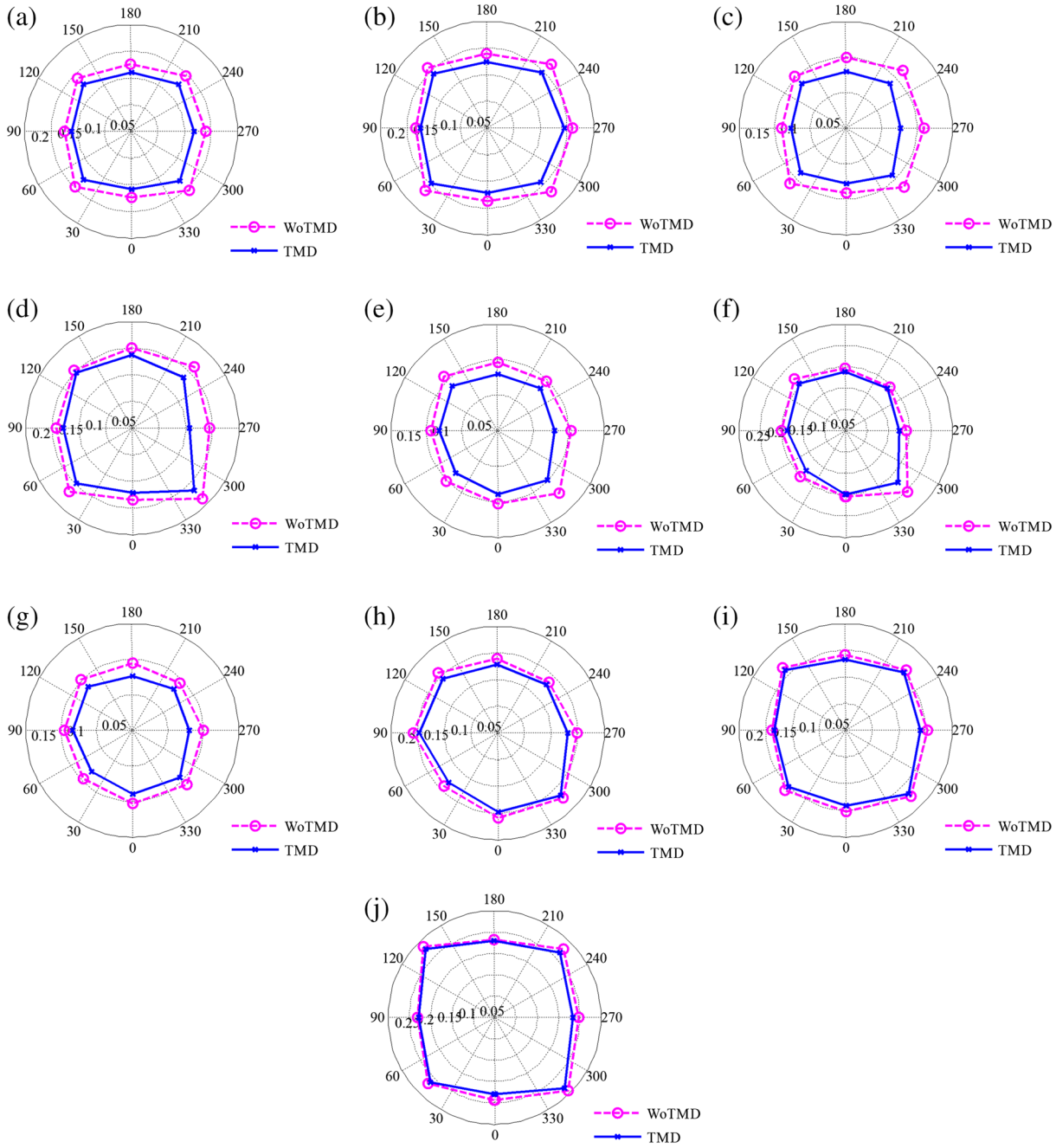

FIGURE 10 Horizontal accelerations of the viewing platform subjected to wind loads with different directions (Unit: m/s^2): (a) Mean accelerations (T1). Horizontal accelerations of the viewing platform subjected to wind loads with different directions (Unit: m/s^2): (b) Maximum accelerations (T1). Horizontal accelerations of the viewing platform subjected to wind loads with different directions (Unit: m/s^2): (c) Mean accelerations (T2). Horizontal accelerations of the viewing platform subjected to wind loads with different directions (Unit: m/s^2): (d) Maximum accelerations (T2). Horizontal accelerations of the viewing platform subjected to wind loads with different directions (Unit: m/s^2): (e) Mean accelerations (T3). Horizontal accelerations of the viewing platform subjected to wind loads with different directions (Unit: m/s^2): (f) Maximum accelerations (T3). Horizontal accelerations of the viewing platform subjected to wind loads with different directions (Unit: m/s^2): (g) Mean accelerations (T4). Horizontal accelerations of the viewing platform subjected to wind loads with different directions (Unit: m/s^2): (h) Maximum accelerations (T4). Horizontal accelerations of the viewing platform subjected to wind loads with different directions (Unit: m/s^2): (i) Mean accelerations (T5). Horizontal accelerations of the viewing platform subjected to wind loads with different directions (Unit: m/s^2): (j) Maximum accelerations (T5). T, tower; TMD, tuned mass damper; WoTMD, responses without TMD

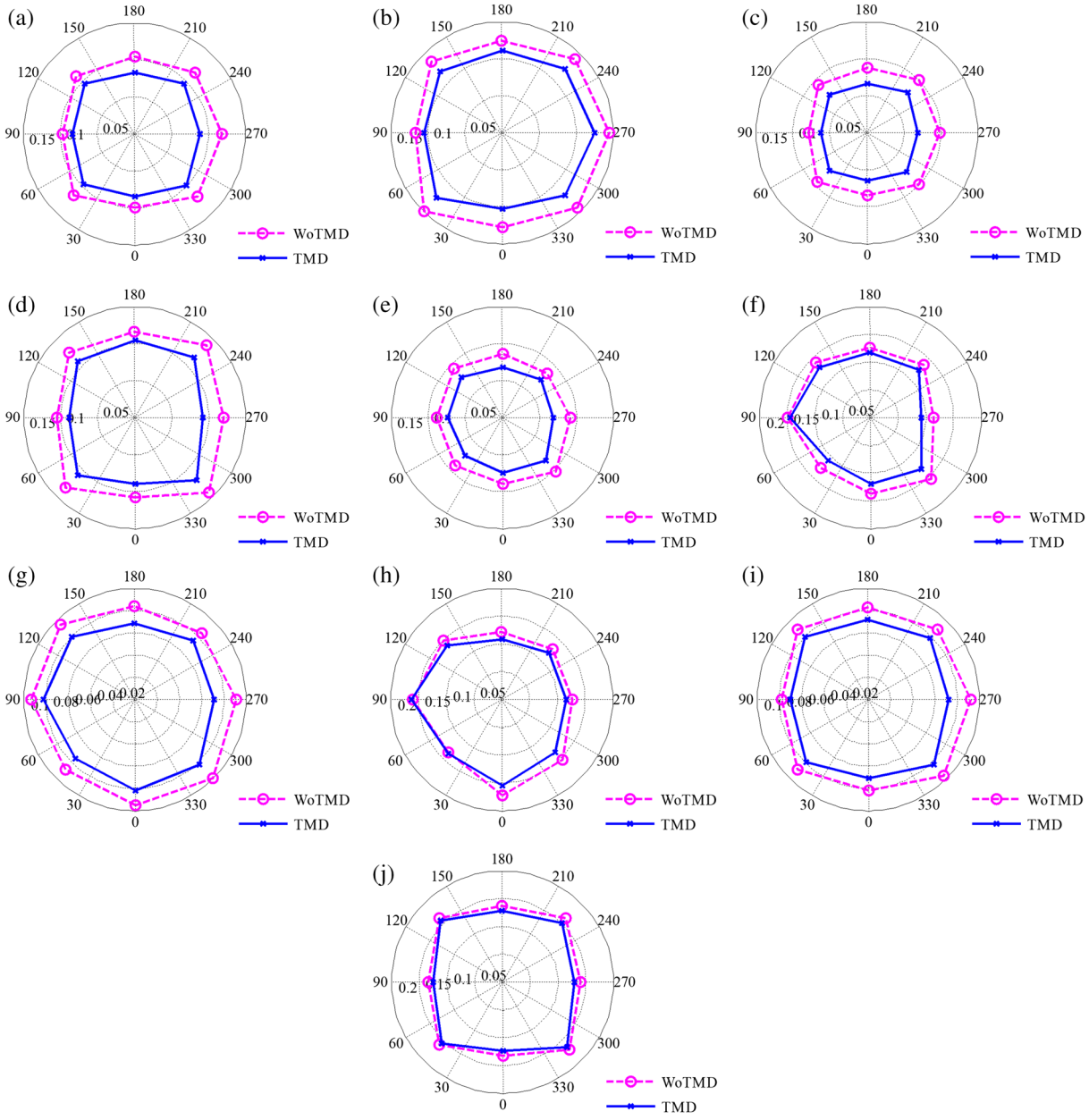

FIGURE 11 Horizontal accelerations of the viewing hall subjected to wind loads with different directions (Unit: m/s^2): (a) Mean accelerations (T1). Horizontal accelerations of the viewing hall subjected to wind loads with different directions (Unit: m/s^2): (b) Maximum accelerations (T1). Horizontal accelerations of the viewing hall subjected to wind loads with different directions (Unit: m/s^2): (c) Mean accelerations (T2). Horizontal accelerations of the viewing hall subjected to wind loads with different directions (Unit: m/s^2): (d) Maximum accelerations (T2). Horizontal accelerations of the viewing hall subjected to wind loads with different directions (Unit: m/s^2): (e) Mean accelerations (T3). Horizontal accelerations of the viewing hall subjected to wind loads with different directions (Unit: m/s^2): (f) Maximum accelerations (T3). Horizontal accelerations of the viewing hall subjected to wind loads with different directions (Unit: m/s^2): (g) Mean accelerations (T4). Horizontal accelerations of the viewing hall subjected to wind loads with different directions (Unit: m/s^2): (h) Maximum accelerations (T4). Horizontal accelerations of the viewing hall subjected to wind loads with different directions (Unit: m/s^2): (i) Mean accelerations (T5). Horizontal accelerations of the viewing hall subjected to wind loads with different directions (Unit: m/s^2): (j) Maximum accelerations (T5). T, tower; TMD, tuned mass damper; WoTMD, responses without TMD

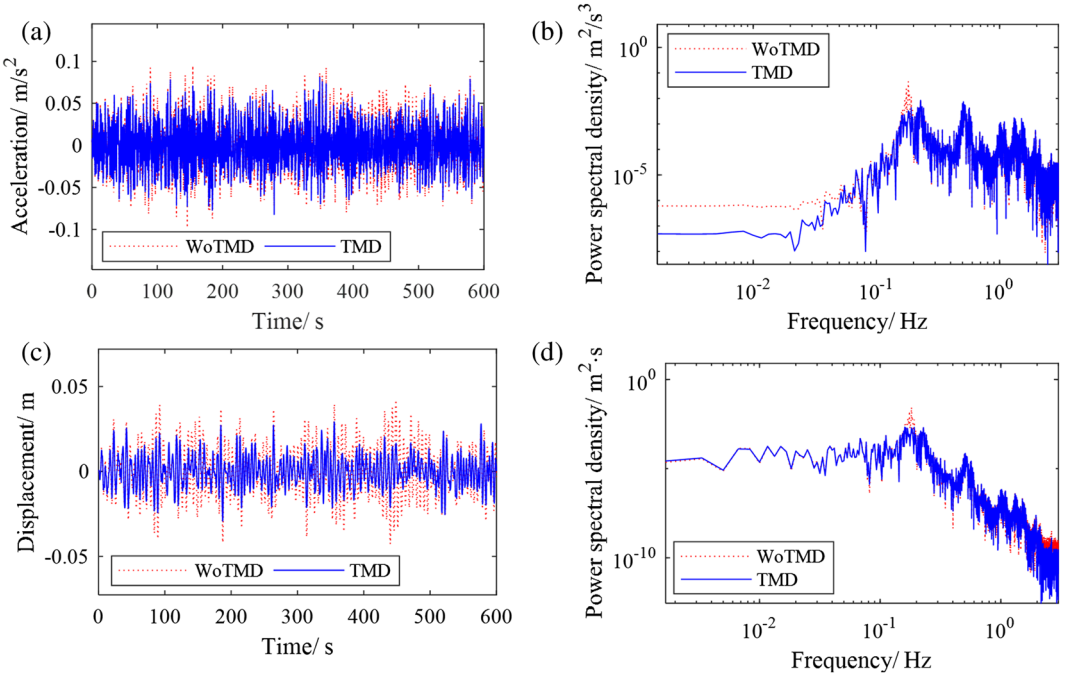

FIGURE 12 Responses in X direction of a point on the viewing platform of Tower 1: (a) Acceleration time history. Responses in X direction of a point on the viewing platform of Tower 1: (b) Acceleration power spectrum density. Responses in X direction of a point on the viewing platform of Tower 1: (c) Displacement time history. Responses in X direction of a point on the viewing platform of Tower 1: (d) Displacement power spectrum density. TMD, tuned mass damper; WoTMD, responses without TMD

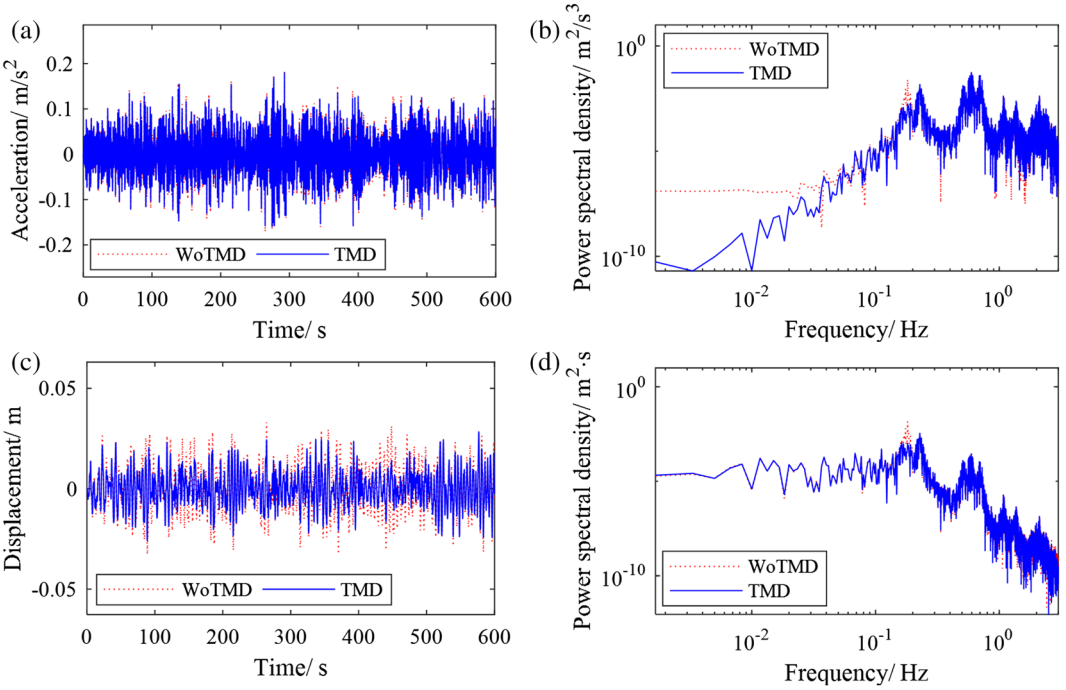

FIGURE 13 Responses in the X direction of a point on the viewing platform of Tower 5: (a) Acceleration time history. Responses in the X direction of a point on the viewing platform of Tower 5: (b)b Acceleration power spectrum density. Responses in the X direction of a point on the viewing platform of Tower 5: (c) Displacement time history. Responses in the X direction of a point on the viewing platform of Tower 5: (d) Displacement power spectrum density. TMD, tuned mass damper; WoTMD, responses without TMD

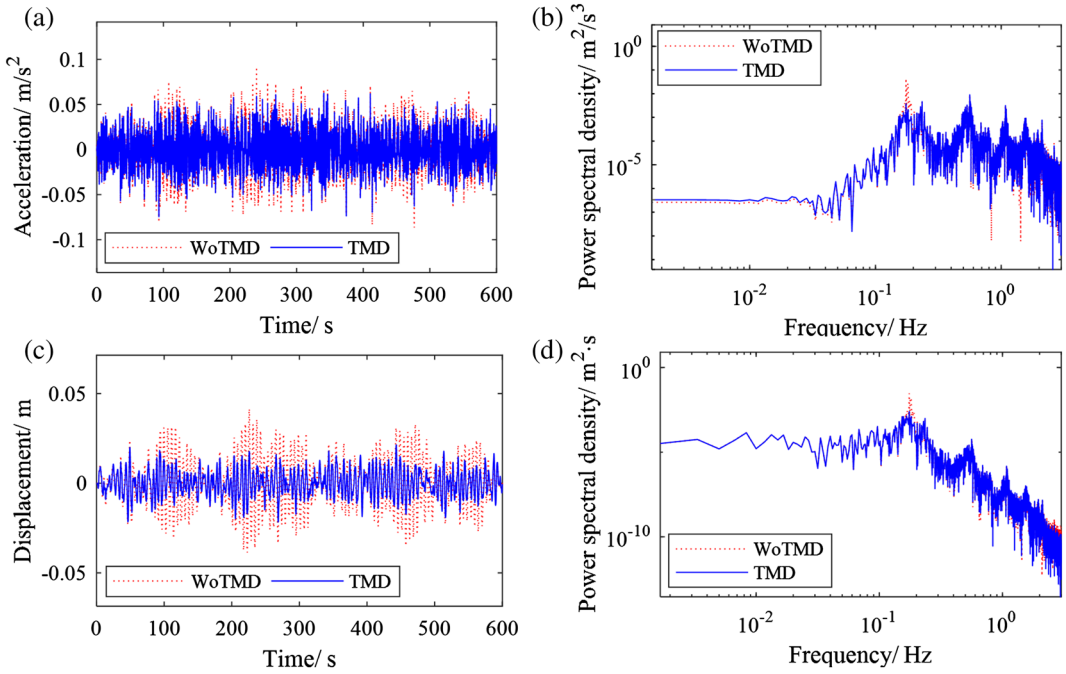

FIGURE 14 Responses in Y direction of a point on the viewing platform of Tower 1: (a) Acceleration time history. Responses in Y direction of a point on the viewing platform of Tower 1: (b) Acceleration power spectrum density. Responses in Y direction of a point on the viewing platform of Tower 1: (c) Displacement time history. Responses in Y direction of a point on the viewing platform of Tower 1: (d) Displacement power spectrum density. TMD, tuned mass damper; WoTMD, responses without TMD

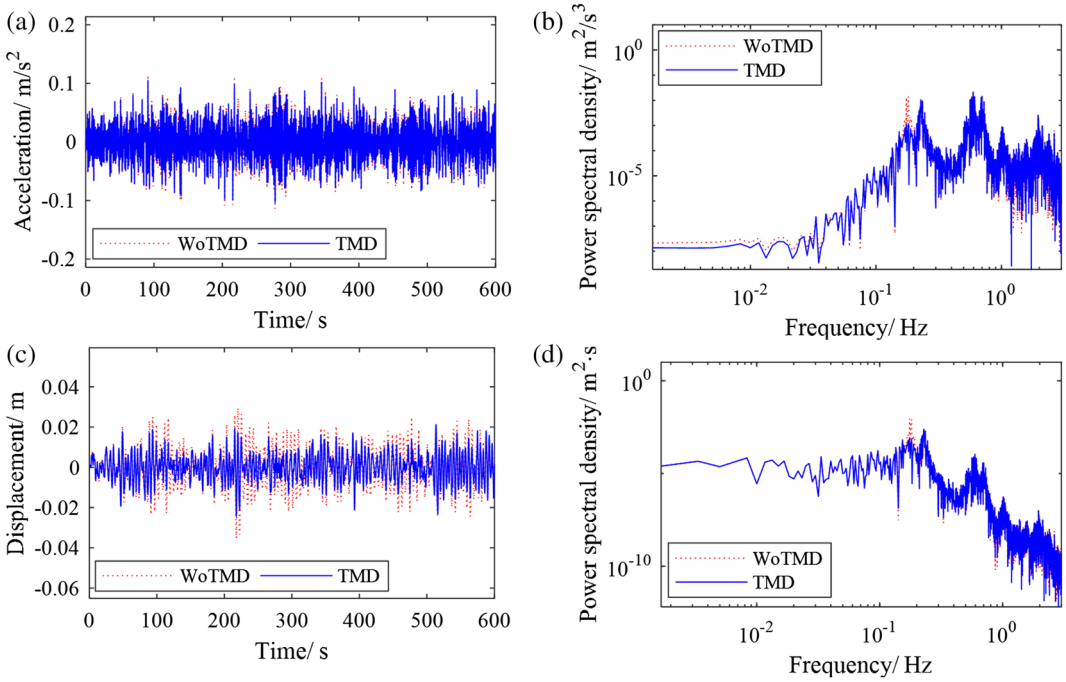

FIGURE 15 Responses in the Y direction of a point on the viewing platform of Tower 5: (a) Acceleration time history. Responses in the Y direction of a point on the viewing platform of Tower 5: (b) Acceleration power spectrum density. Responses in the Y direction of a point on the viewing platform of Tower 5: (c) Displacement time history. Responses in the Y direction of a point on the viewing platform of Tower 5: (d) Displacement power spectrum density. TMD, tuned mass damper; WoTMD, responses without TMD

corresponding damping ratios are 0.120 and 0.116, respectively. Considering the uncertainty in the construction, one can adjust the length of the cables after the field testing.

5.2 | Numerical simulation of the wind-induced vibration

5.2.1 | Spatial distribution

The wind-induced vibrations of the BOT with and without the TMD are analyzed by inputting the three-dimensional wind field simulated in Section 4.2 to the FEM model. Figure 9 shows the spatial distribution of the maximum node acceleration over time under the wind directions of 45 and 135°. The combination of the horizontal accelerations and of all the three acceleration components are $\sqrt{a_x^2 + a_y^2}$ and $\sqrt{a_x^2 + a_y^2 + a_z^2}$, in which a_x, a_y, and a_z are the maximum node accelerations over time in the directions of x, y, and z. It can be observed that (a) the acceleration distributions of the BOT with and without TMD are similar. After the installation of the TMD, the total horizontal accelerations are all reduced. However, the TMD does not affect the vertical acceleration responses. (b) In general, the acceleration increases from the bottom to the top and from the inner part to the outer part. The accelerations of the tower crown are larger than those of the body, especially in the vertical direction. The maximum accelerations the main bodies of the Tower2 and Tower4 are larger than those of the other sub towers, whereas the crowns of the Tower3 and Tower5 are larger than the other towers.

5.2.2 | Response variation with wind directions

There are two main public scenic sites in each sub tower: one is the viewing platform at the top of each tower, and the other is the viewing hall, which is the floor immediately below the platform. As there will be many people on these sites that watch the scenery of Beijing, the issue of human comfort is of concern. Therefore, by considering eight typical wind directions, the mean and maximum horizontal accelerations of the viewing platform and hall are assessed and shown in Figures 10 and 11. It can be concluded from Figure 10 that (a) in general the maximum acceleration occurs at the edge nodes of the viewing platform. The structural constraint on these nodes is much weaker than those at the middle. Thus, the reduction effect of the TMD on the mean accelerations is better than on the maximum accelerations. (b) The wind-induced accelerations of the tower subjected to the wind loads with the directions of 45, 135, 225, and 315° are larger than those subjected to the wind loads with the other directions. This phenomenon is mainly due to the first two modal shapes of the BOT. (c) The best reduction effect is with the wind direction of 270°, when the reduction ratio of Tower1, Tower2, and Tower3 are 16.44, 30.05, and 22.63%, respectively. (d) Because the DPTMD was installed only on Tower1, it has a slight effect on some of the sub towers, among which reduction effect on Tower5 is limited. The reduction effect in the viewing hall as shown in Figure 11 is similar to the effect in the viewing platform. Moreover, the maximum reduction ratio of the viewing hall is 24.56%, which also occurs in the wind direction of 270°. As the connections between Tower1 and Tower5 are weaker than those between Tower1 and the other sub towers, the acceleration reduction effect, both in the viewing platform and in the viewing hall of Tower5, is the weakest among these sub towers. Moreover, the reduction effect in the viewing hall is much better than in the viewing platform.

5.2.3 | Response time history and PSD

The time history responses and the corresponding power spectral densities of two nodes on the viewing platform of Tower1 and Tower5 in the x-direction are shown in Figures 12 and 13 with the wind direction of 45°. Meanwhile, these responses in the y-direction are shown in Figures 14 and 15. In the time domain, the reduction of the displacements is better than the accelerations at both x and y directions. In the frequency domain, the DPTMD has a considerable reduction effect on both the accelerations and displacements at the first bending mode but does not affect the higher modes. However, the higher modes do have some influences on the wind-induced responses, and the accelerations are affected much more than the displacements. Comparing with the node in Tower 5, the reduction effect of the node in Tower1 is much better, and this confirms the conclusions from the analysis in the section above.

6 | CONCLUDING REMARKS

The wind-induced response of the BOT and the performance of its vibration control are presented in this paper. The three-dimensional wind loading for the FEM analysis of the BOT is established based on the wind tunnel test results. Moreover, based on the dynamic characteristics and

responses of the BOT, a DPTMD was designed and installed on the tower. Then, the wind-induced responses of the tower with and without DPTMD are compared with respect to various wind directions and both in the time and frequency domains. Based on the results and discussions presented, the following remarks can be obtained:

1. Mostly, the wind-induced accelerations of the tower subjected to the wind loads with the directions of 45, 135, 225, and 315° are larger than those with the other directions.
2. The DPTMD design utilizes a shorter pendulum length to achieve a long period; thus, a lot of spatial space can be saved given the excellent control performance on the BOT can be ensured. The design serves as a reference for other slender high-rise towers.
3. Only with 0.058% structural mass does the DPTMD mitigate the wind-induced vibration of the tower effectively. The maximum acceleration reduction ratio for the mean accelerations of each floor, which occurs in Tower2 with the wind direction of 270°, reaches 30.05%. Because of the relatively weak connections between sub towers, the reduction effect of the Tower5 is lower than the other sub towers.
4. Because of the limitation of the physical space, only one TMD with a small mass can be installed in this tower. Only the response induced by the first two modes can be suppressed, although higher modes can affect the towers' wind-induced accelerations as well.

ACKNOWLEDGMENTS

The support from the Natural Science Foundation of China under Grant No. 51408389, the Natural Science Foundation of Jiangsu Province under Grant No. BK20161581 and BK20181078, the Six Talent Climax Foundation of Jiangsu under Grant No. JZ-004, the Natural Science Foundation of Jiangsu Education Department under Grant No. 19KJA430019, Jiangsu Government Scholarship for Overseas Studies, and a Project Funded by the Priority Academic Program Development of Jiangsu Higher Education Institutions are gratefully acknowledged.

ORCID

Xin Chen https://orcid.org/0000-0003-1284-5150

REFERENCES

[1] A. K. Ghorbani-Tanha, A. Noorzad, M. Rahimian, *Struc. Design. Tall. Spec. Build.* **2009**, *18*(4), 371.
[2] Y. Kim, K. You, H. Kim, *Struc. Design. Tall. Spec. Build.* **2008**, *17*(3), 669.
[3] B. Chen, D. Yang, Y. Zheng, K. Feng, Y. Ouyang, *Int. J. Struct. Stab. Dyn.* **2018**, *18*(11).
[4] Q. S. Li, L. H. Zhi, A. Y. Tuan, C. S. Kao, S. C. Su, C. F. Wu, *J. Struct.l Eng.-ASCE* **2011**, *137*(1), 143.
[5] A. Kareem, T. Kijewski, Y. Tamura, *Wind Struct.* **1999**, *2*(3), 201.
[6] B. Basu, O. S. Bursi, F. Casciati, S. Casciati, A. E. del Grosso, M. Domaneschi, L. Faravelli, J. Holnicki-Szulc, H. Irschik, M. Krommer, M. Lepidi, A. Martelli, B. Ozturk, F. Pozo, G. Pujol, Z. Rakicevic, J. Rodellar, *Struct. Control Health Monit.* **2014**, *21*(12), 1414.
[7] G. W. Housner, L. A. Bergman, T. K. Caughey, A. G. Chassiakos, R. O. Claus, S. F. Masri, R. E. Skelton, T. T. Soong, B. F. Spencer, J. T. P. Yao, *J. Eng. Mech.* **1997**, *123*(9), 897.
[8] Y. Ikeda, *Struct. Control Health Monit.* **2009**, *16*(7-8), 703.
[9] T. T. Soong, B. F. Spencer, *Eng. Struct.* **2002**, *24*(3), 243.
[10] B. F. Spencer, S. Nagarajaiah, *J. Struct.l Eng.-ASCE* **2003**, *129*(7), 845.
[11] X. Chen, Y. Ding, Z. Zhang, P. Sun, A. Q. Li, *Earthq. Eng. Eng. Vib.* **2012**, *11*(1), 57.
[12] K. Ohtake, Y. Mataki, T. Ohkuma, J. Kanda, H. Kitamura, *J Wind Eng Ind Aerod* **1992**, *41-44*, 2225.
[13] T. Nagase, T. Hisatoku, *Struct. Des. Tall Build.* **1992**, *1*, 35.
[14] A. J. Roffel, S. Narasimhan, T. Haskett, *J. Struct.l Eng.-ASCE* **2013**, *139*(12), 04013019.
[15] T. Saito, K. Shiba, K. Tamura, *Earth. Eng. Struct. D.* **2001**, *30*(11), 1677.
[16] L. L. Chung, L. Y. Wu, K. H. Lien, H. H. Chen, H. H. Huang, *Struct. Control Health Monit.* **2013**, *20*(4), 544.
[17] Z. Lu, B. Huang, Q. Zhang, X. Lu, *J. Sound Vib.* **2018**, *421*, 153.
[18] A. Sarkar, O. T. Gudmestad, *Eng. Struct.* **2013**, *49*, 221.
[19] G. B. Song, P. Zhang, L. Y. Li, M. Singla, D. Patil, H. N. Li, Y. L. Mo, *J. Eng. Mech.* **2016**, *142*(6), 04016031.
[20] P. Zhang, G. Song, H. N. Li, Y. X. Lin, *J. Eng. Mech.* **2013**, *139*(10), 1395.
[21] J. P. Den Hartog, *Mechanical vibrations*, McGraw-Hill, New York **1956** 492.
[22] C. C. Chang, W. L. Qu, *Struc. Design. Tall. Spec. Build.* **1998**, *7*(2), 147.
[23] F. Sadek, B. Mohraz, A. W. Taylor, R. M. Chung, *Earthq Eng. Struc. Dynam.* **1997**, *26*(6), 617.
[24] G. B. Warburton, *Earthq Eng. Struc. Dynam.* **1982**, *10*(3), 381.
[25] L. L. Chung, L. Y. Wu, C. S. W. Yang, K. H. Lien, M. C. Lin, H. H. Huang, *Struct. Control Health Monit.* **2013**, *20*(3), 320.
[26] Y. Z. Fujino, M. Abe, *Earthq Eng. Struc. Dynam.* **1993**, *22*(10), 833.
[27] N. Hoang, Y. Fujino, P. Warnitchai, *Eng. Struct.* **2008**, *30*(3), 707.
[28] G. Bekdaş, S. M. Nigdeli, *Eng. Struct.* **2011**, *33*(9), 2716.
[29] G. Bekdaş, S. M. Nigdeli, X. Yang, *Eng. Struct.* **2018**, *159*, 89.
[30] G. Carlo Marano, R. Greco, B. Chiaia, *J. Sound Vib.* **2010**, *329*(23), 4880.
[31] A. Farshidianfar, S. Soheili, *IJOCE* **2013**, *3*(3), 409.
[32] X. Jin, S. Xie, J. He, Y. Lin, Y. Wang, N. Wang, *Ocean Eng.* **2018**, *167*, 130.
[33] A. Y. T. Leung, H. Zhang, C. C. Cheng, Y. Y. Lee, *Earthq Eng. Struc. Dynam.* **2008**, *37*(9), 1223.

[34] Q. An, Z. Chen, Q. Ren, H. Liu, X. Yan, *J. Constr. Steel Res.* **2015**, *115*, 359.
[35] Hancock Tower now to get dampers. (**1975**). Engineering News Records, 11.
[36] C. Kao, A. Y. Tuan, Q. S. Li, *J. Struc. Eng.* **2011**, *137*(1), 143.
[37] Z. Zhou, X. Wei, Z. Lu, B. Jeremic, *Struct. Design Tall Spec. Build.* **2018**, *27*(14), e1501.
[38] N. Kang, H. Kim, S. Choi & Seongwoo Jo, J. S. Hwang, E. Yu, *Comput. Aided Civ. Inf. Eng.* **2012**, *27*(6), 455.
[39] R. J. McNamara, *J. Struct. Divis.* **1977**, *103*(9), 1785.
[40] BeijingInternational. (**2016**). Permanent olympic symbol marks beijing's new landmark<http://www.ebeijing.gov.cn/feature_2/SportsinBeijing/t1438765.htm>. June, 19,2019.
[41] OlympicNews (**2016**). Olympic rings join the Beijing skyline <https://www.olympic.org/news/olympic-rings-join-the-beijing-skyline>. June, 19th,2019.
[42] G. Ming, P. Huang, L. Tao, X. Zhou, Z. Fan, *J. Fluid. Struct.* **2010**, *26*(7-8), 1142.
[43] GB50009-2012, *Load code for design of building structures*, China Architecture & Building Press, Beijing **2012**.

How to cite this article: Chen X, Li A, Zhang Z, et al. Improving the wind-induced human comfort of the Beijing Olympic Tower by a double-stage pendulum tuned mass damper. *Struct Design Tall Spec Build*. 2020;29:e1704. https://doi.org/10.1002/tal.1704